Perica Paunović[1]
Faculty of Technology and Metallurgy,
SS Cyril and Methodius University,
Rudjer Bošković, 16,
Skopje 1000, Republic of Macedonia
e-mail: pericap@tmf.ukim.edu.mk

Anita Grozdanov
Faculty of Technology and Metallurgy,
SS Cyril and Methodius University,
Rudjer Bošković Str., 16,
Skopje 1000, Republic of Macedonia
e-mail: anita@tmf.ukim.edu.mk

Andrej Češnovar
OKTA Crude Oil Refinery AD,
Skopje 1000, Republic of Macedonia
e-mail: cesnovar.andrej@gmail.com

Petre Makreski
Institute of Chemistry,
Faculty of Natural Sciences and Mathematics,
SS Cyril and Methodius University,
Arhimedova Str., 5,
Skopje 1000, Republic of Macedonia

Gennaro Gentile
Institute for Chemistry and
Technology of Polymers,
National Research Council,
Fabricato Oliveti 70,
Pozzuoli, Napoli 80078, Italy
e-mail: gengenti@ictp.cnr.it

Bogdan Ranguelov
Institute of Physical Chemistry,
Bulgarian Academy of Sciences,
Acad.G.Bonchev Str., Bl.11,
Sofia 1113, Bulgaria
e-mail: rangelov@ipc.bas.bg

Emilija Fidančevska
Faculty of Technology and Metallurgy,
SS Cyril and Methodius University,
Rudjer Bošković Str., 16,
Skopje 1000, Republic of Macedonia
e-mail: emilijaf@tmf.ukim.edu.mk

Characterization of Nanoscaled TiO_2 Produced by Simplified Sol–Gel Method Using Organometallic Precursor

This work is concerned with development of sol–gel method for preparation of nanoscaled TiO_2 using organometallic precursor—titanium tetraisopropoxide (TTIP) and determination of the present crystalline phases depending on the temperature of further thermal treatment. The characteristic processes and transformations during the thermal treatment were determined by means of thermal gravimetric analysis and/or differential thermal analysis (TGA/DTA) method. The crystalline structure and size of the TiO_2 crystallites were analyzed by means of Raman spectroscopy and X-ray powder diffraction (XRPD) method. At 250 °C, cryptocrystalline structure was detected, where amorphous TiO_2 is accompanied with crystalline anatase. The anatase crystallite phase is stable up to 650 °C, whereas at higher temperature rutile transformation begins. It was observed that at 800 °C, almost the whole TiO_2 is transformed to rutile phase. According to XRPD analysis, the increase of the temperature influences on the increase of the size of the crystalline particles ranging from 6 nm at 250 °C to less than 100 nm at 800 °C. The size and shape of the TiO_2 crystalline particles were observed by transmission electron microscopy (TEM). The shape of the studied samples changes from nanospheres (250, 380, and 550 °C) to nanorods (650 and 800 °C). Morphology of the formed TiO_2 aggregates was observed by scanning electron microscopy (SEM).
[DOI: 10.1115/1.4029112]

Introduction

Titania, the naturally occurring oxide of titanium, is an inexpensive, innocuous, stable and environmentally friendly material with wide range of technical and technological applications such as catalyst (for chemical, photochemical, and electrocatalysis), pigment, optical devices, sensor, sunblocking material in cosmetics, binder in medicine, etc. [1–7]. This is the result of its favorable physical and chemical properties, and variety of crystalline forms in which exists. In nature, TiO_2 occurs in three forms—rutile, anatase, and brookite. The most thermodynamically stable is rutile, whereas brookite and anatase are metastable and transform to rutile upon heating [7–9].

Recently, the nanostructured materials with their unique physical properties (mechanical, optical, catalytic, etc.), entirely different from those of the conventional micro- or milli-meter sized materials, offer wider, and more effective applications. In this context, all crystallographic forms of nanosized TiO_2 particles are of great importance and interest within the modern science and engineering application. Because these properties are structure- and size-dependent, it is important to develop new routes of synthesis by which the crystalline structure, the size, and the shape of TiO_2 nanocrystals can be readily manipulated.

Many different methods have been developed and applied for the preparation of nanosized TiO_2 particles. Methods such as sol–gel [10,11], microemulsion or reverse micelles [12,13], hydrothermal [14–17] and solvothermal [18,19] synthesis, direct oxidation method [20,21], chemical vapor deposition (CVD) [22], and

[1]Corresponding author.

Contributed by the Materials Division of ASME for publication in the Journal of Engineering Materials and Technology. Manuscript received October 6, 2013; final manuscript received November 8, 2014; published online December 15, 2014. Assoc. Editor: Vadim V. Silberschmidt.

microwave radiation [23,24] have all been used for the preparation of nano-TiO_2 particles.

Crystalline TiO_2 nanoparticles were synthesized by Zhang et al. [13] by hydrolysis of titanium tetrabutoxide in the presence of acids (hydrochloric acid, nitric acid, sulfuric acid, and phosphoric acid) in NP-5 (Igepal CO-520)-cyclohexane reverse micelles at room temperature. Many groups have used the hydrothermal method to prepare TiO_2 nanoparticles [15,16]. Usually, the hydrothermal synthesis was conducted in steel autoclaves with or without Teflon liners under controlled temperature and/or pressure with the reaction in aqueous solutions. It is a method that was widely used for the production of small particles in the ceramics industry. The solvothermal method is almost identical to the hydrothermal method except that the solvent used here is nonaqueous [18]. However, the temperature was elevated much higher than the reported one in hydrothermal method, since a variety of organic solvents with high boiling points can be chosen. The solvothermal method has better control over the hydrothermal methods considering the size, shape distributions, and crystallinity of the TiO_2 nanoparticles. The solvothermal method has been employed to synthesize TiO_2 nanoparticles and nanorods with/without the aid of surfactants [18,19]. TiO_2 nanomaterials were also obtained either by direct oxidation of titanium metal using oxidants or under anodization. Crystalline TiO_2 nanorods have been obtained by direct oxidation of a titanium metal plate with hydrogen peroxide [20,21]. The formation of crystalline TiO_2 occurs through a dissolution precipitation mechanism. The crystalline phase (anatase or rutile) of TiO_2 nanorods can be controlled by the addition of inorganic salts of NaX ($X = F^-$, Cl^-, and SO_4^{2-}). Using the CVD method, thick crystalline TiO_2 films with grain sizes below 30 nm as well as TiO_2 nanoparticles with sizes below 10 nm can be prepared by pyrolysis of TTIP in a mixed helium/oxygen atmosphere, using liquid precursor delivery [22]. Microwave radiation is applied to prepare various TiO_2 nanomaterials [23,24]. Corradi et al. found that colloidal TiO_2 nanoparticles suspensions could be prepared within 5 min to1 h with microwave radiation, while 1–32 h was needed for the conventional synthesis method of forced hydrolysis at 195 °C [23]. Wu et al. synthesized TiO_2 nanotubes by microwave radiation via the reaction of TiO_2 crystals of anatase, rutile, or mixed phase and NaOH aqueous solution under a certain microwave power. Usually, the TiO_2 nanotubes had the central hollow, open-ended, and multiwall structure with diameters of 8–12 nm and lengths up to 200–1000 nm [24].

In comparison to the other methods, the sol–gel route is considered as a very promising method for the synthesis of ultrafine metallic oxide [25] and has been widely applied for preparation of TiO_2 nanoparticles [26,27]. This process normally proceeds via an acid-catalyzed hydrolysis step of titanium(IV) alkoxide followed by condensation. The development of Ti–O–Ti chains is favored with low content of water, low hydrolysis rates, and excess titanium alkoxide in the reaction mixture. Several different precursors can be used for sol–gel synthesis route, for example, TTIP, $TiCl_4$, etc. [28].

The aim of this study is the application and development of a sol–gel procedure for producing nanosized TiO_2 from TTIP acting as an organometallic precursor.

Experimental

The investigated TiO_2 samples were prepared by sol–gel procedure simplified in some parts by the present authors. As a precursor for preparation of TiO_2, TTIP (Aldrich, 97%) was used. TTIP was dissolved in anhydrous ethanol (Merck, p.a.) in the ratio Ethanol:TTIP = 8:1. To provide hydrolysis of TTIP to $Ti(OH)_4$, small amount of 1 M HNO_3 was added in the ratio TTIP:HNO_3 = 10:1. This mixture was evaporated at 65 °C and ambient pressure with continuous stirring with 600–900 rpm. Hydrolysis process occurs according the following reaction:

$$Ti(OCH(CH_3)_2)_4 + 4H_2O \rightarrow Ti(OH)_4 + 4(CH_3)_2CH(OH)$$

Final product of the sol–gel synthesis was a fine nanoscaled powder of $Ti(OH)_4$ with light-yellow color. The produced light-yellow powder of $Ti(OH)_4$ after sol–gel procedure was studied by means of TGA, DTA, and derivative thermogravimetry (DTG), in order to identify changes caused by increasing the temperature. TGA/DTA measurements were performed using a Perkin Elmer PYRIS Diamond Thermogravimetric/Differential Thermal Analyzer. 20 mg of the studied material were heated in the temperature interval of 25 °C–1000 °C by heating rate of 10 °C·min^{-1} in nitrogen atmosphere. The temperatures of the further thermal treating were chosen according to the characteristic points determined by TGA/DTA analysis. The working temperatures of the thermal treatments were 20–30 °C above the determined points.

To decompose $Ti(OH)_4$ into TiO_2 and to remove the residual amount of organic groups, the powder was heated for 2 h in chamber furnace in the air atmosphere at different working temperatures: 250, 380, 550, 650, and 800 °C.

Identification of the structure of present phases was performed by Raman spectroscopy and XRPD. Nonpolarized Raman spectra were recorded on micro-Raman multichannel spectrometer Horiba JobinYvon LabRam 300 Infinity. The Raman effect was excited by 632.8 nm laser line from a He:Ne laser. To avoid burning of the samples, the laser power was reduced to 0.11 mW/cm^2 by the use of a filter. An Olympus MPlanN confocal microscope with-$\times$ 100 objective for magnification was used. The spectral resolution was set to 4 cm^{-1}. In order to focus the laser beam, a confocal hole of about 2 μm was used and the position on the sample surface was adjusted using motorized x–y stage. The Raman shift was calibrated using the Raman peak of silica located at 520.7 cm^{-1}. The acquisition time and the accumulation were set to 5 s and 15 scans, respectively. XRPD measurements were carried out by X-ray powder diffractometer Philips APD 15, with Cu$K\alpha$ radiation. The diffraction data were collected at a constant rate of 0.02 deg·s^{-1} over an angle range of 2θ from 10 deg to 90 deg. The average crystallite size was calculated from the broadening of the XRPD peaks using the Scherrer's equation [29].

TEM observation of the prepared samples was performed by using a Transmission Electron Microscope—FEI Tecnai G2 Spirit TWIN equipped with LaB6. Further, they were observed by SEM microscopy, while the surface composition was determined by means of energy dispersive spectroscopy (EDS). For this purpose, Scanning Electron Microscope JEOL 6390 with EDS Oxford Inca Energy 350 was used.

Results and Discussions

TGA/DTA Analysis. Characteristic curves of the thermal analysis such as TGA, DTA, and DTG are shown separately in Figs. 1–3.

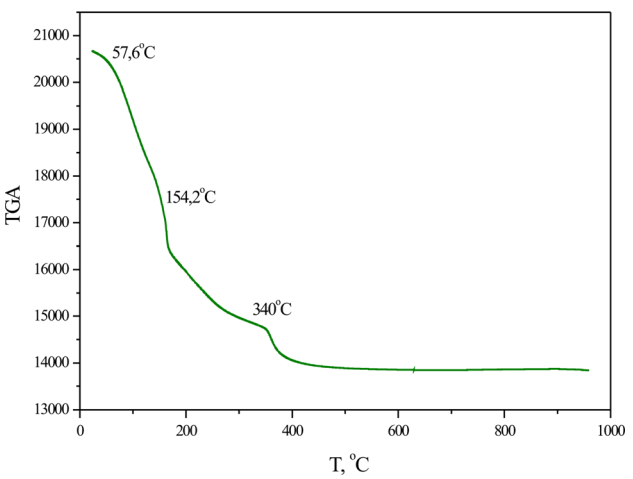

Fig. 1 TGA curve of the $Ti(OH)_4$ produced after sol–gel procedure

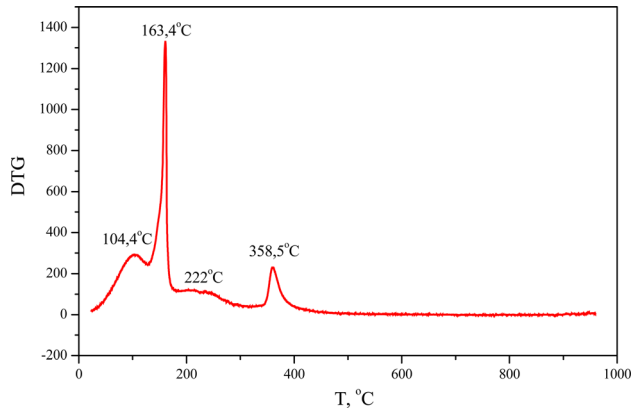

Fig. 2 DTG curve of the $Ti(OH)_4$ produced after sol–gel procedure

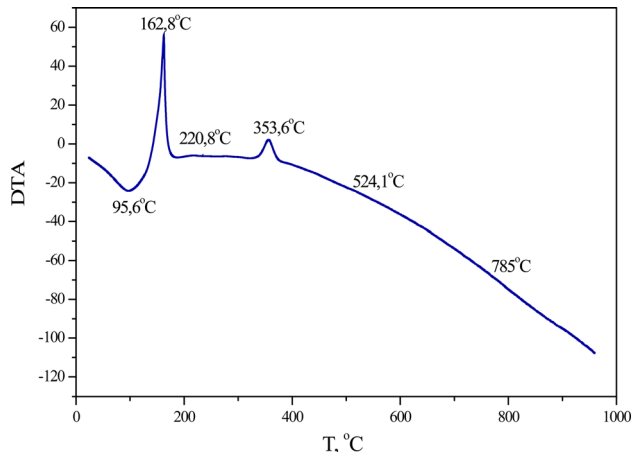

Fig. 3 DTA curve of the $Ti(OH)_4$ produced after sol–gel procedure

Table 1 Characteristic DTG and DTA transformation points

DTG characteristic points (°C)	DTA characteristic points (°C)
104.4	95.6
163.2	162.8
222	220.8
358.5	353.6
	524.1
	785

The weight losses due to the physicochemical transformations in $Ti(OH)_4$ occurred gradually and exhibit three characteristic points in the TGA curve (at 57,6; 154,2, and 340 °C). The first weight loss below 100 °C usually corresponds to physical or chemical desorption of the species such as H_2O (dehydration) and CO_2 (vaporizing of the organic residues in the sample). The main weight loss of about 32% occurred in the range from 100 to 500 °C. The second and the third TGA points correspond to the well defined endothermic peaks in DTA curve (at 162.8 °C and 353.4 °C) and DTG curve (163.4 °C and 358.5 °C). All detected peaks in DTA and DTG curves are summarized in the Table 1.

The endothermic peak at 95.6 °C which corresponds to DTG peak at 104.4 °C is due to the evaporation of physically adsorbed water in the studied samples as result of the air contact. This is in agreement with the literature data [30,31]. The second point in the range of 162.8 °C (DTA) and 163.2 °C (DTG curve) is due to the complete desorption of the surface adsorbed water as well as on the beginning of the decomposition of the organic residual precursor groups of TTIP.

In the range of 220.8 °C, DTA curve (222 °C DTG curve) exhibits broad maximum with plateau that could be related to the complete decomposition of the organic residues and start of removal of OH^- groups (dehydroxylation) [32] indicating that TiO_2 formation is starting. In order to define precisely this phase transformation, Raman spectra and XRPD patterns were recorded confirming that, in this range, anatase was found, which is in accordance with literature data [33].

The next exothermic maximum in the range of 353.6 °C (DTA) and 358.5 °C (DTG) without weight loss, suggests complete decomposition of OH^- groups (dehydroxylation). Also, this peak can be attributed to the phase transformation of cryptocrystalline TiO_2 to crystalline anatase.

Further increase of the temperature contributes to the monotonous decrease of the DTA curve and two detected characteristic points at 524.1 °C and 785 °C. According to Lee et al. [33], between 450 °C and 800 °C, transformation of anatase to rutile phase undergoes and the difference in the transformation temperature depends on the precursor type, the preparation conditions of the particles, and the properties of particles. So, these critical points can be correlated with the start of crystalline transformation of anatase to rutile phase [33].

For more detailed analysis of the detected TGA/DTA/DTG points, further Raman spectroscopy and XRPD analyses were performed.

Raman Analysis. The Raman spectra of the studied samples are shown in Fig. 4. As it can be seen, the Raman spectra for the samples thermally treated at 250, 380, 550, and 650 °C show smooth baseline (except the sloped one of the sample treated at 250 °C). In addition, the positions of each characteristic Raman peak (having the same band width) clearly identify the TiO_2 samples as anatase. The sloped and rugged spectrum of the sample treated at 250 °C points out its lower crystallinity compared to those treated at higher temperatures [34]. These peaks correspond to the well-known spectrum of anatase single crystal identified by Oshaka [35], but with slightly broader and shifted Raman maxima. These spectra are consisted of the following Raman vibration modes symmetry types: 3 E_g positioned at 144, 197, and 639 cm^{-1}, B_{1g} positioned at 399 cm^{-1} and doublet of A_{1g} and B_{1g} registered at 514 cm^{-1}. The wavenumbers of the Raman modes detected in the samples are presented in Table 2. As the temperature of the thermal treatment increases, slight shift of the corresponding active Raman modes to lower wavenumbers can be observed, especially pronounced for the strongest Raman peak

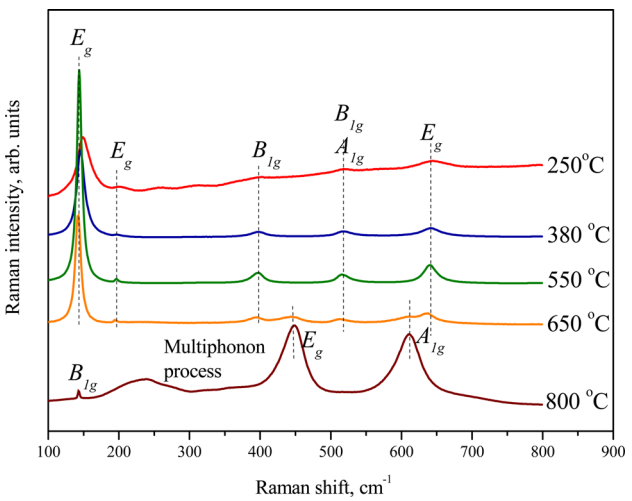

Fig. 4 Raman spectra of TiO_2 produced by thermal treatment of $Ti(OH)_4$ at different temperatures

Table 2 Position of the characteristic bands from Raman spectra of the studied samples

	Temperature of thermal treatment (°C)	E_g (cm^{-1})	E_g, cm^{-1}	B_{1g} (cm^{-1})	A_{1g}, B_{1g} (cm^{-1})	E_g (cm^{-1})
1.	250	148.9	199.7	402.2	518.7	643.5
2.	380	145.3	196.7	397.7	518	641
3.	550	144.1	196.4	397.1	516	640.3
4.	650	143.8	196.1	396.8	515.4	639.9

	Temperature of thermal treatment (°C)	B_{1g}, (cm^{-1})	Multiphoton process (cm^{-1})	E_g (cm^{-1})	A_{1g} (cm^{-1})
4.	650	—	—	443.4	609.08
5.	800	142.9	236.8	448.6	610.45

($148.9\,cm^{-1}$ compared to $142.8\,cm^{-1}$). This shift and broadening of the Raman bands can be described by phonon confinement model [36,37]—decrease of the particle size causes confinement of the phonon within the particle and consequently, the phonon momentum distribution increases. This phonon dispersion causes broadening and may lead to a shift of the Raman bands. On the other hand, the shift and broadening of the Raman bands can be affected by nonstoichiometric defects due to oxygen deficiency within the material [34,38]. However, in our case, the conditions of the thermal treatment of the studied samples (oxidative atmosphere) are not favorable for creation of oxygen vacancies. Also, the results of the EDS analysis (in all samples the weight and atomic Ti:O ratio were ~59.81:40.19 and 66.79:33.21, respectively) indicating that the contribution of oxygen in all samples is not less than the theoretical one that confirm the absence of oxygen deficiency. According to these statements, the shift of the Raman bands can be ascribed to the increase of the phonon dispersion as result of decreasing of the particles size. The increase of the temperature during the thermal treatment causes increasing of the particles size and consequently, decreasing of the wavenumbers of the corresponding Raman peaks.

Raman spectrum of the sample thermally treated at 800 °C (Fig. 4) shows Raman bands at 142.9, 448.6, and $610.45\,cm^{-1}$ corresponding to B_{1g}, E_g, and A_{1g} symmetry modes of rutile single crystal, respectively [39]. The band at $236.8\,cm^{-1}$ corresponds to the multiphoton process characteristic for rutile crystal structure of TiO_2 [40] (see Table 2). Despite the appearance of all characteristic peaks for rutile crystals in the spectrum of the sample treated at 800 °C, a weak band evolved at $142.9\,cm^{-1}$ serving as an indicator for subtle presence of anatase, since the peak for the reported mode (with E_g symmetry) is the strongest one in the Raman spectrum of the latter TiO_2 analog. Therefore, it is most likely that this sample either contains residual amount of anatase crystal structure or resembles to pure rutile crystals, if consider this band as B_{1g} mode in rutile.

Very weak bands characteristic for rutile (E_g and A_{1g}) can be seen in the spectrum of the sample treated at 650 °C. However, the Raman spectrum implies that the anatase occurs as a dominant phase (strongest peaks in the spectrum), associated by small presence of rutile (weak and wide bands from rutile also appear).

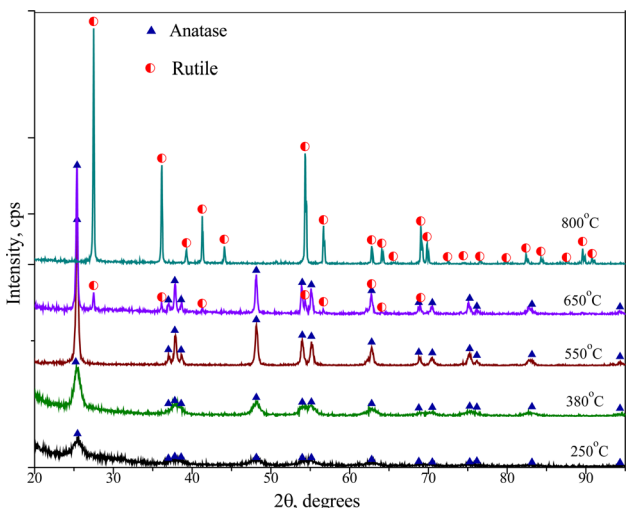

Fig. 5 XRPD patterns of TiO_2 produced by thermal treatment of $Ti(OH)_4$ at different temperatures

XPRD Analysis. To clear this ambiguity as well as to clarify the corresponding transformations detected by characteristic DTA points, XRPD analysis was performed.

XRPD patterns of the studied TiO_2 samples are shown in Fig. 5. As the temperature of thermal treatment of samples decreases, the diffraction peaks became broader. XRPD debyegram of the sample treated at 250 °C shows the broadest diffraction peaks with scattered character. This indicates the presence of amorphous TiO_2. On the other hand, characteristic diffraction peaks are detected at several positions within this spectrum. Thus, we can consider that this sample shows cryptocrystalline structure [41,42]. Therefore, the broad maximum with plateau in the range of 220.8 °C in DTA curve (222 °C DTG curve), besides due to the complete decomposition of the organic residues, can be ascribed to formation of amorphous TiO_2 and its further crystallization into anatase. XRPD patterns of the samples treated at 380 and 550 °C are less broad than the previous one and all registered peaks indicate the presence of anatase. The slight scattered character of spectrum of the sample treated at 380 °C is an indicator for residual amorphous phase in this sample. Thus, the exothermic peak in the range of 353.6 °C (DTA) and 358.5 °C (DTG), suggests only complete decomposition of OH^- groups (dehydroxylation), but not and complete transformation of cryptocrystalline TiO_2 to crystalline anatase. Complete transformation to crystalline anatase occurs at 524.1 °C (detected DTA point). XRPD debyegram of the sample treated at 550 °C is well shaped with sharp and narrower peaks characteristic for anatase. Transformation to rutile phase was not detected. The spectrum of the sample treated at 650 °C indicates higher crystallinity than the previous samples, but now, with obvious presence of rutile phase. The small presence of rutile phase was detected also in corresponding Raman spectrum. Finally, the sample treated at 800 °C shows well shaped XRPD pattern with peaks characteristic for rutile crystalline form of TiO_2. Peaks characteristic for anatase were not detected. According to this observation, it is clear that the Raman band of this sample positioned at $142.9\,cm^{-1}$ is due to the presence of rutile. In addition, we can conclude that at 785 °C (DTA detected point) complete transformation of anatase to rutile occurred. The XRPD patterns are in good correlation with the Raman spectra.

Using the Scherrer's equation, the average crystallite size was calculated from the broadening of the XRPD peaks. The size of the crystallites is shown in Table 3. As the temperature of the thermal treatment increases, the size of the TiO_2 crystallites increases from 6 nm at 250 °C to less than 100 nm at 800 °C.

Table 3 Size of the crystallites of TiO_2 produced at different temperatures

	Temperature of the thermal treatment (°C)	Diameter of the crystallites (nm)
1.	250	6
2.	380	11
3.	550	$15 < d < 25$
4.	650	$35 < d < 45$
5.	800	<100

TEM Analysis. TEM analysis was performed (Fig. 6) to confirm the results regarding the crystalline size of the studied materials obtained by XRPD analysis as well as to determine the shape of the TiO_2 crystallites. At lower temperatures (250, 380, and 500 °C) spherical form of crystallites was observed with size similar to those determined by XRPD analysis whereas formation of rods occurred at 650 °C. The length of the crystallites ranging 35–45 nm and their diameter approaches 12 nm. At 800 °C, well-formed nanorods with length within 50–100 nm and diameter of 25 nm were observed. According to these results, one can

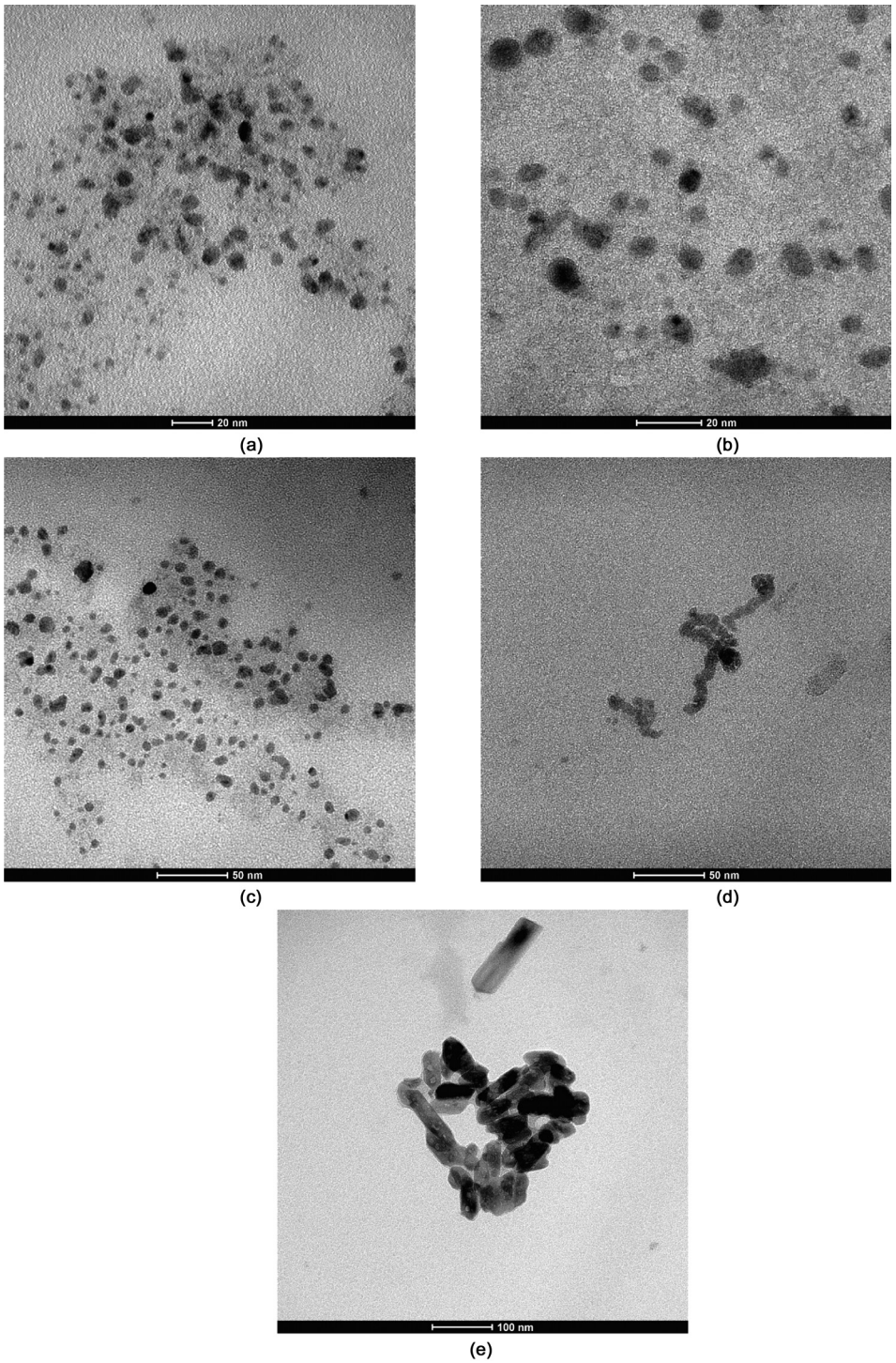

Fig. 6 TEM images of TiO_2 produced by thermal treatment of $Ti(OH)_4$ at (*a*) 250 °C, (*b*) 380 °C, (*c*) 550 °C, (*d*) 650 °C, and (*e*) 800 °C

conclude pronounced correlation between results of crystallite size determined by XRPD and TEM analysis.

SEM Analysis. SEM analysis of the studied samples was performed in order to observe morphology of the produced TiO_2. The samples show similar morphology as seen in Fig. 7. Namely, TiO_2 crystallites form aggregates with irregular geometric shape. Presence of holes and cracks is evident, which contributes to developed active surface area. The holes between particles contribute to increased interparticle porosity, while the cracks contribute to increased transparticle porosity. This is very convenient and suitable for application of these materials for catalytic purposes (photocatalysis, electrocatalysis, etc.). Increased inter- and transparticle porosity provides easier reach of liquid reactants to and removal of gaseous products from the reaction place.

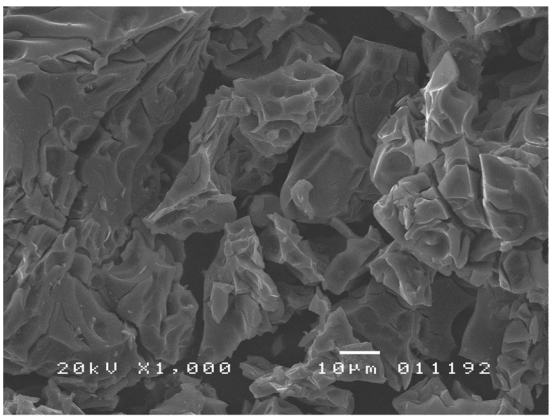

(a)

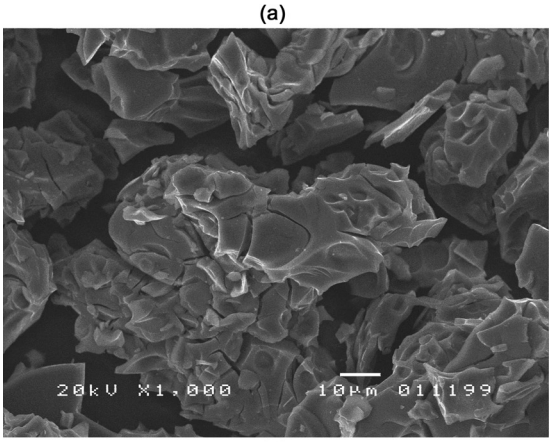

(b)

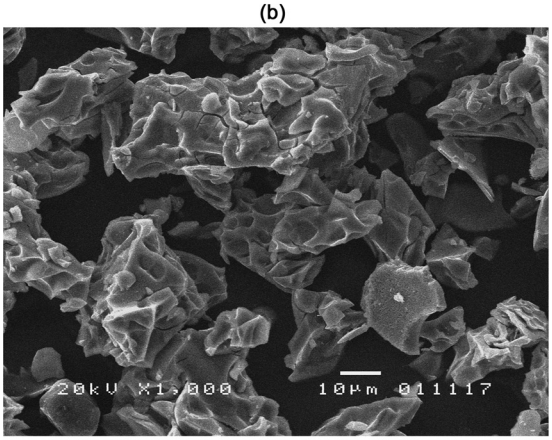

(c)

Fig. 7 SEM images of TiO_2 produced by thermal treatment of $Ti(OH)_4$ at (*a*) 250 °C, (*b*) 380 °C, and (*c*) 800 °C

Conclusion

The research presented in this paper was motivated by the idea to produce nanostructured TiO_2 by sol–gel method in simplified conditions. Furthermore, it enables to apply as a component for improving the activity of electrocatalysts aimed in hydrogen economy as well as in photocatalysis for degradation of the hazard pollutants. According to the exposed results of the TiO_2 characterization, we could draw the following conclusions:

(1) A sol–gel method for preparation of nanoscaled TiO_2 was developed using TTIP as a precursor in simplified conditions: ambient pressure and temperature of 65 °C. The sol–gel produced $Ti(OH)_4$ (yellow powder) further thermally treated at different temperatures in air atmosphere in order to produce different crystalline phases of TiO_2. The temperatures of the thermal treatment were determined by TGA/DTA diagrams: 20–30 °C above the determined characteristic DTA points.

(2) Characteristic physicochemical transformations during the heating of the sol–gel produced $Ti(OH)_4$ were determined by means of TGA/DTA analysis.
Decomposition of the organic residual precursor groups of TTIP started at 162.8 °C and fully finished at 220.8 °C, while complete decomposition of OH^- groups (dehydroxylation) occurred at 353.6 °C.
As the temperature of the thermal treatment increases, TiO_2 structure above 222 °C changes from cryptocrystalline to completely pure anatase (at 524.1 °C). Above 650 °C an existing of two phases—anatase and rutile were detected, while at 785 °C transformation of anatase to rutile was completed. Above 785 °C pure rutile phase exists.

(3) The size of crystallites increases by increase of the temperature in the following order: spherical nanoparticles of 6 nm at 250 °C, 11 nm at 380 °C, 15–25 nm at 550 °C, and nanorods of 35–45 nm in length and 12 nm in diameter at 650 °C and nanorods of 50 to less than 100 nm in length and 12 nm in diameter at 800 °C.

(4) The studied samples show similar morphology of the formed aggregates—irregular geometric shape of the aggregates with presence of holes and cracks. The holes between particles contribute to increased interparticle porosity, while the cracks contribute to increased transparticle porosity which is suitable for application of these materials for catalytic purposes.
The determined characteristics of the studied materials point out that they can be used as catalytic materials and further research will be focused on their application in photocatalysis for degradation of organic pollutants and in electrocatalysis as a component of electrocatalysts aimed for hydrogen electrolysers/fuel cells.

Acknowledgment

This paper has been supported by and carried out within the project Synthesis, Characterization and Application of Nanoscaled Non-stoichiometric Titanium Oxides—Magneli Phases, Ministry of Education and Science of R. Macedonia (Agreement No. 13-3576/2, Oct. 27, 2010).

References

[1] Matsuda, S., and Kato, A., 1983, "Titanium Oxide Based Catalysts—A Review," Appl. Catal., **8**(2), pp. 149–165.
[2] Tauster, S. J., Fung, S. C., and Garten, R. L., 1978, "Strong Metal-Support Interactions. Group 8 Noble Metals Supported on Titanium Dioxide," J. Am. Chem. Soc., **100**(1), pp. 170–175.
[3] Frank, S. N., and Bard, A. J., 1977, "Heterogeneous Photocatalytic Oxidation of Cyanide and Sulfite in Aqueous Solutions at Semiconductor Powders," J. Phys. Chem., **81**(15), pp. 1484–1488.
[4] Trasatti, S., 1994, "Transition Metal Oxides: Versatile Materials for Electrocatalysis," *Electrochemistry of Novel Materials*, J. Lipkowski and P. N. Ross, eds., VCH, New York.

[5] Mezey, E. J., 1966, "Pigments and Reinforcing Agents," *Vapor Deposition*, C. F. Powell, J. H. Oxley, and J. M. Blocher, eds., Wiley, New York.
[6] Reithmaier, J. P., Paunović, P., Kulish, W., Popov, C., and Petkov, P., eds., 2011, *Nanotechnological Basis for Advanced Sensors*, Springer, Dordrecht, The Netherlands.
[7] Diebold, U., 2003, "The Surface Science of Titanium Dioxide," Surf. Sci. Rep., **48**(5–8), pp. 53–229.
[8] Navrotsky, A., and Kleppa, O., 1967, "Enthalpy of the Anatase–Rutile Transformation," J. Am. Ceram. Soc., **50**(11), p. 626.
[9] Zhang, H., and Banfield, J., 2000, "Understanding Polymorphic Phase Transformation Behavior During Growth of Nanocrystalline Aggregates: Insights From TiO_2," J. Phys. Chem. B, **104**(15), pp. 3481–3487.
[10] Lal, M., Chhabra, V., Ayyub, P., and Maitra, A., 1998, "Preparation and Characterization of Ultrafine TiO_2 Particles in Reverse Micelles by Hydrolysis of Titanium Di-Ethylhexyl Sulfosuccinate," J. Mater. Res., **13**(5), pp. 1249–1254.
[11] Selvaraj, U., Prasadrao, A. V., Komerneni, S., and Roy, R., 1992, "Sol–Gel Fabrication of Epitaxial and Oriented TiO_2 Thin Films," J. Am. Ceram. Soc., **75**(5), pp. 1167–1170.
[12] Bacsa, R. R., and Grätzel, M., 1996, "Rutile Formation in Hydrothermally Crystallized Nanosized Titania," J. Am. Ceram. Soc., **79**(8), pp. 2185–2188.
[13] Zhang, D., Qi, L., Ma, J., and Cheng, H., 2002, "Formation of Crystalline Nanosized Titania in Reverse Micelles at Room Temperature," J. Mater. Chem., **12**(12), pp. 3677–3680.
[14] Kutty, T. R. N., Vivekanandan, R., and Murugaraj, P., 1988, "Precipitation of Rutile and Anatase (TiO_2) Fine Powders and Their Conversion to $MTiO_3$ (M = Ba, Sr, Ca) by the Hydrothermal Method," Mater. Chem. Phys., **19**(6), pp. 533–546.
[15] Andersson, M., Oesterlund, L., Ljungstroem, S., and Palmqvist, A., 2002, "Preparation of Nanosize Anatase and Rutile TiO_2 by Hydrothermal Treatment of Microemulsions and Their Activity for Photocatalytic Wet Oxidation of Phenol," J. Phys. Chem. B, **106**(41), pp. 10674–10679.
[16] Yang, J., Mei, S., and Ferreira, J. M. F., 2001, "Hydrothermal Synthesis of TiO_2 Nanopowders From Tetraalkylammonium Hydroxide Peptized Sols," Mater. Sci. Eng. C, **15**(1–2), pp. 183–185.
[17] Kasuga, T., Hiramatsu, M., Hoson, A., Sekino, T., and Niihara, K., 1998, "Formation of Titanium Oxide Nanotube," Langmuir, **14**(12), pp. 3160–3163.
[18] Li, X. L., Peng, Q., Yi, J. X., Wang, X., and Li, Y. D., 2006, "Near Monodisperse TiO_2 Nanoparticles and Nanorods," Chem. Eur. J., **12**(8), pp. 2383–2391.
[19] Yang, S. W., and Gao, L., 2006, "Fabrication and Shape-Evolution of Nanostructured TiO_2 Via a Sol–Solvothermal Process Based on Benzene–Water Interfaces," Mater. Chem. Phys., **99**(2–3), pp. 437–440.
[20] Wu, J. M., Hayakawa, S., Tsuru, K., and Osaka, A., 2002, "Porous Titania Films Prepared From Interactions of Titanium With Hydrogen Peroxide Solution," Scr. Mater., **46**(1), pp. 101–106.
[21] Wu, J. M., and Zhang, T. W., 2004, "Photodegradation of Rhodamine B in Water Assisted by Titania Films Prepared Through a Novel Procedure," Photochem. Photobiol. A, **162**(1), pp. 171–177.
[22] Seifried, S.,Winterer, M., and Hahn, H., 2000, "Nanocrystalline Titania Films and Particles by Chemical Vapor Synthesis," Chem. Vap. Deposition, **6**(5), pp. 239–244.
[23] Corradi, A. B., Bondioli, F., Focher, B., Ferrari, A. M., Grippo, C., Mariani, E., and Villa, C., 2005, "Conventional and Microwave-Hydrothermal Synthesis of TiO_2 Nanopowders," J. Am. Ceram. Soc., **88**(9), pp. 2639–2641.
[24] Wu, X., Jiang, Q. Z., Ma, Z. F., Fu, M., and Shangguan, W. F., 2005, "Synthesis of Titania Nanotubes by Microwave Irradiation," Solid State Commun., **136**(9–10), pp. 513–517.
[25] Li, B., Wang, X., Yan, M., and Li, L., 2002, "Preparation and Characterization of Nano-TiO_2 Powder," Mater. Chem. Phys., **78**(1), pp. 184–188
[26] Hague, M. J., and Mayo, D. C., 1994, "Controlling Crystallinity During Processing of Nanocrystalline Titania," J. Am. Ceram. Soc., **77**(7), pp. 1957–1960.
[27] Mehrizad, A., Gharbani, P., and Tabatabii, S. M., 2009, "Synthesis of Nanosized TiO_2 Powder by Sol–Gel Method in Acidic Conditions," J. Iran. Chem. Res., **2**(2), pp. 145–149.
[28] Samsonov, G. V., 1982, *The Oxide Handbook*, IFI/Plenum Press, New York.
[29] Cullity, B. D., 1978, *Elements of X-Ray Diffraction*, Addison-Wesley, London, UK.
[30] So, W. W., Park, S. B., Kim, K. J., Shin, C. H., and Moon, S. J., 2001, "The Crystalline Phase Stability of Titania Particles Prepared at Room Temperature by the Sol–Gel Method," J. Mater. Sci., **36**(17), pp. 4299–4305.
[31] Mehranpour, H., Askari, M., Ghamsari, M. S., and Farzalibeik, H., 2010, "Study on the Phase Transformation Kinetics of Sol–Gel Drived TiO_2 Nanoparticles," J. Nanomater., **2010**, p. 626978.
[32] Holgado, M., Cintas, A., Ibisate, M., Serna, C. J., Lopez, C., and Meseguer, F., 2000, "Three-Dimensional Arrays Formed by Monodisperse TiO_2 Coated on SiO_2 Spheres," J. Colloid Interface Sci., **229**(1), pp. 6–11.
[33] Lee, M. S., Lee, G. D., Park, S. S., and Hong, S. S., 2003, "Synthesis of TiO_2 Nanoparticles in Reverse Microemulsion and Their Photocatalytic Activity," J. Ind. Eng. Chem., **9**(1), pp. 89–95.
[34] Lei, Y., Zhang, L. D., and Fan, J. C., 2001, "Fabrication, Characterization and Raman Study of TiO_2 Nanowire Arrays Prepared by Anodic Oxidative Hydrolysis of $TiCl_3$," Chem. Phys. Lett., **338**(4–6), pp. 231–236.
[35] Oshaka, T., Izumi, F., and Fujiki, Y., 1978, "Raman Spectrum of Anatase, TiO_2," J. Raman Spectrosc., **7**(6), pp. 321–324.
[36] Xu, C. Y., Zhang, P. X., and Yan, L., 2001, "Blue Shift of Raman Peak From Coated TiO_2 Nanoparticles," J. Raman Spectrosc., **32**(10), pp. 862–865.
[37] Choi, H. C., Jung, Y. M., and Kim, S. B., 2005, "Size Effects in the Raman Spectra of TiO_2 Nanoparticles," Vib. Spectrosc., **37**(1), pp. 33–38.
[38] Parker, J. C., and Siegel, R. W., 1990, "Raman Microprobe Study of Nanophase TiO_2 and Oxidation-Induced Spectral Changes," J. Mater. Res., **5**(6), pp. 1246–1252.
[39] Porto, S. P. S., Fleury, P. A., and Damen, T. C., 1966, "Raman Spectra of TiO_2, MgF_2, ZnF_2, FeF_2, and MnF_2," Phys. Rev., **154**(2), pp. 522–526.
[40] Ma, H. L., Yang, J. Y., Dai, Y., Zhang, Y. B., Lu, B., and Ma, G. H., 2007, "Raman Study of Phase Transformation of TiO_2 Rutile Single Crystal Irradiated by Infrared Femtosecond Laser," Appl. Surf. Sci., **253**(18), pp. 7497–7500.
[41] Xie, Y., and Yuan, C., 2004, "Photocatalysis of Neodymium Ion Modified TiO_2 Sol Under Visible Light Irradiation," Appl. Surf. Sci., **221**(1–4), pp. 17–24.
[42] Xie, Y., and Yuan, C., 2004, "Visible Light Induced Photocatalysis of Cerium Ion Modified Titania Sol and Nanocrystallites," J. Mater. Sci. Technol., **20**(1), pp. 14–18.